

## STARS GET DIZZY AFTER LUNCH

MICHAEL ZHANG

Department of Astrophysical Sciences, 5491 Frist Center, Princeton University, Princeton, NJ 08544, USA

KALOYAN PENEV

Department of Astrophysical Sciences, 4 Ivy Lane, Peyton Hall, Princeton University, Princeton, NJ 08544, USA

*Draft version March 8, 2021*

### ABSTRACT

Exoplanet searches have discovered a large number of ‘hot Jupiters’—high-mass planets orbiting very close to their parent stars in nearly circular orbits. A number of these planets are sufficiently massive and close-in to be significantly affected by tidal dissipation in the parent star, to a degree parametrized by the tidal quality factor  $Q_*$ . This process speeds up their stars’ rotation rate while reducing the planets’ semimajor axis. In this paper, we investigate the tidal destruction of hot Jupiters. Because the orbital angular momenta of these planets are a significant fraction of their stars’ rotational angular momenta, they spin up their stars significantly while spiralling to their deaths. Using Monte Carlo simulation, we predict that for  $Q_* = 10^6$ ,  $3.9 \times 10^{-6}$  of stars with the Kepler Target Catalog’s mass distribution should have a rotation period shorter than 1/3 day (8 h) due to accreting a planet. Exoplanet surveys such as SuperWASP, HATnet, HATsouth, and KELT have already produced light curves of millions of stars. These two facts suggest that it may be possible to search for tidally-destroyed planets by looking for stars with extremely short rotational periods, then looking for remnant planet cores around those candidates, anomalies in the metal distribution, or other signatures of the recent accretion of the planet.

### 1. INTRODUCTION

Counselman (1973) showed that a planet-satellite system evolving under tidal dissipation has three outcomes: the satellite could spiral inwards to its death, spiral outwards to escape, or approach a tidally locked equilibrium. Ever since the discovery of the first exoplanets, astronomers have studied tidal decay due to exoplanet-star interactions. For example, Rasio et al. (1996) studied tidal dissipation in 51 Pegasi b—the first exoplanet discovered around a main-sequence star—and concluded that the planet’s orbit is unstable, even though the decay time is longer than its star’s main-sequence lifetime. Most of the early exoplanets were similar to 51 Pegasi b—they are hot Jupiters, with high masses and short orbital periods.

Tidal decay in planetary systems has been relied on to explain a wide variety of phenomena. For example, it is hypothesized to be responsible for circularizing eccentric orbits—although this is due to tides in the planet, not in the star. The standard theory of hot Jupiter formation suggests they formed outside the ice line and migrated closer to their stars by one or both of two mechanisms: interaction with the protoplanetary disk or with other planets. At this early age, the star’s rotation frequency would be faster than the planet’s orbital frequency and increasing due to shrinking of the star, so tidal forces would act to push the planet outwards and prevent it from spiralling into the star (Plavchan & Bilinski (2013)). Tidal decay has also been implicated in the apparent correlation between high obliquity, as measured by the Rossiter-McLaughlin effect, and high stellar temperature. The hypothesis is that higher-mass (and hotter) stars have much thinner convective zones, and are thus subject to much less tidal

dissipation. A lower-mass star would have a significant convective zone, causing a massive planet’s orbit to significantly evolve towards alignment (Winn et al. (2010)). More recently, Albrecht et al. (2012) examined a larger set of RM measurements and found that the temperature dependence in Winn et al. (2010) still holds. Additionally, they found that obliquity is smaller for hot Jupiters where the expected tidal timescale is short, consistent with a hot Jupiter formation mechanism where the planets’ initial obliquity is random.

Depending on the tidal dissipation efficiency, massive hot Jupiters close to their stars may spiral in towards the Roche limit and be destroyed in a short timespan, depositing their angular momentum on the star’s envelope while leaving behind a small, rocky, low-period core. Jackson et al. (2013) carried out a search for extremely low-period transiting objects in the Kepler dataset and found 13 candidates, with periods from 3.3 to 10 hours and estimated masses from 3-200 Earth masses (with large error bars). The authors suggest the possibility that these objects are the remnants of destroyed hot Jupiters. Teitler & Königl (2014) investigated the phenomenon discovered by McQuillan et al. (2013)—namely, the dearth of Kepler Objects of Interest (KOIs) with orbital periods smaller than 2-3 days around stars with rotation periods shorter than 5-10 days. They use a Monte Carlo model to select an initial population of planets and evolve them forward in time, accounting for tidal interaction, magnetic braking, and core-envelope coupling. The authors conclude that the observed distribution of low orbital period, low rotation period systems is qualitatively consistent with the simulated distribution if  $Q_*$  is around  $10^5$  to  $10^6$ .

At least two examples of tidal destruction may have

already been discovered. Adamów et al. (2012) reports the discovery of BD+48740, a star with unusually high lithium content and with a  $1.6 M_J$  planet in a highly eccentric ( $e \approx 0.67$ ) orbit. The authors suggest that both characteristics—both unusual for an evolved star—can be explained by the recent engulfment of a more inner planet. They also note that current data is not accurate enough to verify this hypothesis. Jackson et al. (2010) examines CoRot-7b, the first confirmed rocky exoplanet, and suggests that it could have originated as a farther-out gas giant, after which evaporation and tidal decay reduced it to its current state.

Metzger et al. (2012) found that the destruction of a hot Jupiter might be observable on a human timescale. The authors predict that destruction happens at a galactic rate of  $0.1 - 1 \text{ yr}^{-1}$ , and describe 3 qualitatively different scenarios, depending on the planet-to-star density ratio  $\rho_p/\rho_*$ . If  $\rho_p/\rho_* > 5$ , the planet plunges directly into the star, creating a EUV/soft x-ray transient that lasts weeks to months and an optical transient lasting days. If  $\rho_p/\rho_* < 1$ , the planet reaches the Roche radius and stably transfers mass to its star over a timescale of 1000 years—the most difficult scenario to observe. If  $1 < \rho_p/\rho_* < 5$ , the planet is disrupted into an accretion disk, which causes an optical transient that lasts weeks to months. Optical transients are expected to be similar to, but distinguishable from, classical novae.

This paper takes a parallel course to Metzger et al. (2012) and estimates the fraction of Sun-like stars in the galaxy that have swallowed a planet and are rotating at extremely short rotation periods ( $P < 8h$ ) as a result. Extreme rotation periods might be good tracers for planet death because few stars, especially on the main sequence, naturally spin this fast. Exoplanet surveys such as SuperWASP (Street & SuperWASP Consortium (2004)), HATnet (Bakos et al. (2004)), HATsouth (Bakos et al. (2013)), and KELT (Pepper et al. (2007)) have produced light curves of millions of stars to detect planetary transits. Light curves produced by these surveys are ideal for finding short-rotation-period stars. 8h is much shorter than the orbital periods of the planets that the surveys routinely detect, and starspots are not likely to change significantly over 8h, giving a very highly periodic photometric signal. The question of how many stars amongst these millions have detectable rotation periods is addressed in Section 4.2.

To make this estimate, we need to know the tidal dissipation efficiency. Unfortunately, the tidal dissipation efficiency is very poorly known, and proposed values range from  $10^6 - 10^{12}$  (Barker & Ogilvie (2009)). Depending on the value of  $Q_*$ , the planet could have a significant effect on the star’s rotation rate, or it could have a negligible effect for the entirety of the star’s lifetime. Data on the circularization of binary stellar orbits seem to indicate  $Q_* \approx 10^5$  or  $Q_* \approx 10^6$  (Meibom & Mathieu (2005)). However, Ogilvie & Lin (2007) propose that hot Jupiters should have smaller dissipation efficiency than binary stars because the Hough waves they excite are not damped at the center of the star. Penev & Sasselov (2011) also argue that there is good reason to suspect that  $Q_*$  may not be  $10^6$  for planet-hosting stars due to differences in the mechanism of dissipation. For example, the members of a binary stellar system are likely

to be tidally locked, whereas most known transiting hot Jupiters do not have enough orbital angular momentum to synchronize their stars’ rotation with their orbit.

Numerous planets have been used to constrain  $Q_*$ . Hellier et al. (2009) analyzed WASP-18b, the first discovered planet with a period less than 1 day, and found that a  $Q_*$  of  $10^6$  would mean the planet’s remaining lifetime is less than a thousandth of the star’s main-sequence lifetime, and that the shift in transit timing would be detectable after only 10 years. It should be noted that WASP-18 is a 1.24 solar mass star, and that tidal dissipation may be less efficient in stars of this high mass due to the absence of a convective zone. Hellier et al. (2011) analyze WASP-19b and conclude that likely values for  $Q_*$  are  $10^7 - 10^8$ , but because the age of WASP-19 is highly uncertain, the best estimate being that it has a 65 percent chance of being older than 1 Gyr with estimates ranging from a few hundred Myr to many Gyr (Hebb et al. (2010)), no firm conclusions can be drawn. Penev et al. (2012) argue that the distribution of planet orbital periods is inconsistent with  $Q_* < 10^7$  with 99 percent probability. Because  $Q_*$  is so uncertain, we will run simulations for  $Q_* = 10^6$ ,  $Q_* = 10^7$ , and  $Q_* = 10^8$ .

This paper is divided into 4 further sections. The first, ‘Model’, will describe the set of ODEs we use to model the evolution of a stellar system, as well as our choice of parameters for the ODEs. ‘Simulation method’ will describe the code used to solve these ODEs, the planets chosen for constraining  $Q$ , and the distributions of planetary and stellar parameters used to estimate the number of fast rotators. ‘Results’ has a self-evident name. ‘Conclusions’ will discuss the possibility of detecting planets as they inspiral into their stars and shortly afterwards.

## 2. MODEL

Our model is the same as the one used by Penev et al. (2012). Planets are assumed to be in circular orbits and tidally locked to their stars. Tidal dissipation within the planet itself is therefore negligible. The dynamical evolution of a stellar system is assumed to be governed by the following differential equations:

$$\frac{da}{dt} = \text{sign}(\omega_c - \omega_{orb}) \frac{9}{2} \sqrt{\frac{G}{aM_*}} \left(\frac{R_*}{a}\right)^5 \frac{m_p}{Q_*} \quad (1)$$

$$\left(\frac{dL_c}{dt}\right)_{\text{tide}} = -\frac{1}{2} m_p M_* \sqrt{\frac{G}{a(M_* + m_p)}} \frac{da}{dt} \quad (2)$$

$$\left(\frac{dL_c}{dt}\right)_{\text{wind}} = -K \omega_c \min(\omega_c, \omega_{\text{sat}})^2 \left(\frac{R_*}{R_\odot}\right)^{1/2} \left(\frac{M_*}{M_\odot}\right)^{-1/2} \quad (3)$$

$$\frac{dL_c}{dt} = \frac{\Delta L}{\tau_c} - \frac{2}{3} R_r^2 \omega_c \frac{dM_r}{dt} + \left(\frac{dL}{dt}\right)_{\text{wind}} + \left(\frac{dL}{dt}\right)_{\text{tide}} \quad (4)$$

$$\frac{dL_r}{dt} = -\frac{\Delta L}{\tau_c} + \frac{2}{3} R_r^2 \omega_c \frac{dM_r}{dt} \quad (5)$$

$$\Delta L = \frac{I_c L_r - I_r L_c}{I_c + I_r} \quad (6)$$

where  $a$  is the planet’s semimajor axis,  $M_*$  is the star’s mass,  $m_p$  is the planet’s mass,  $\omega_{orb}$  is the planet’s orbital frequency,  $L_c, I_c, \omega_c$  are the convective zone’s angular momentum, moment of inertia, and rotation rate

respectively,  $I_r, I_r, \omega_r, M_r, R_r$  are the radiative zone’s angular momentum, moment of inertia, rotation rate, mass, and radius respectively, and  $K, \omega_{sat}, \tau_c$  are constants set by the rotation model. The rotation model will be discussed in more detail in the next subsection.

Equation 1 is given by Goldreich (1963); Kaula (1968); Jackson et al. (2008). Equation 2 follows from conservation of momentum, assuming that momentum lost by the planet is added to the star’s convective zone. Equation 3 is taken from Stauffer & Hartmann (1987); Kawaler (1988); Barnes & Sofia (1996), and models the magnetic spindown of the star. Equation 5 uses a formulation by MacGregor (1991) and Allain (1998) to model the interaction between core and envelope, while Equation 4 follows trivially from Equation 5.

The quantities  $I_c, I_r, M_r, R_r$  and  $R_*$  are taken from stellar evolution tracks computed using the YREC model (Demarque et al. (2008)), which contain these quantities at various ages for masses of 0.5, 0.6, 0.7, 0.8, 0.9, 1.0, 1.05, 1.1, 1.15 and  $1.2 M_\odot$ . Cubic spline interpolation was used to interpolate between the ages for each mass, after which another cubic spline interpolation was used to interpolate between masses. Since this interpolation is only valid for  $0.5\text{--}1.2 M_\odot$ , we never simulate stars outside this range anywhere in the paper. Because high-mass stars have thin convective zones, which may cause different physical mechanisms to dominate the tidal dissipation and lead to a different  $Q_*$ , we further restrict ourselves to  $M_* < 1.05 M_\odot$  throughout the paper.

We assume that the planet forms at 5 Myr, and that its orbit does not change by any mechanism except tidal dissipation in the star. This formation scenario is justified if the planet is brought to its initial orbit by disk interaction. It might not be justified if the planet arrives via Kozai resonance or planet-planet scattering, followed by tidal circularization due to tides raised on the planet.

### 2.1. Rotation model

Equation 3 above models angular momentum loss due to the stellar magnetic wind. This model, the same as the one used by Irwin & Bouvier (2009), reproduces Skumanich’s law until  $\omega_{conv} \geq \omega_{sat}$ , at which point the rate of angular momentum loss becomes proportional to the rotation rate as opposed to its cube. In addition to  $\omega_{sat}$ , a planetless star’s rotational evolution depends on two parameters: the magnetic wind strength  $K$ , and the core-envelope coupling timescale  $\tau_c$ .

This paper focuses its attention on stars of  $0.5\text{--}1.05$  solar masses. Stars of this mass initially have a wide distribution of rotation rates. Irwin & Bouvier (2009) compiled 3100 rotation periods of stars in open clusters and found rotation periods ranging from less than 0.1 days to more than 10 days in clusters younger than 5 Myr. This paper, just like Irwin & Bouvier, will assume the convective rotation rate is held constant before the disk dissipates.

We take our values for  $\omega_{sat}$  and  $\tau_c$  from Gallet & Bouvier (2013). They use a different rotation model, but it turns out that our model approximates their model decently well, as shown in Figure 1. Furthermore, they derived their fits by eye, so we do not lose a substantial amount of accuracy.

The authors quote a single value for  $\omega_{sat}$ , namely 10 times the solar rotational frequency, or 2.45 rad/day.

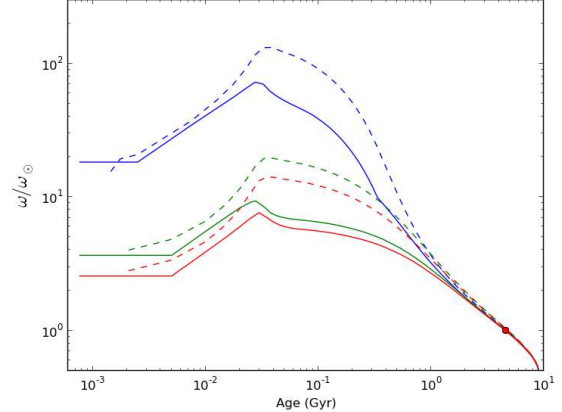


FIG. 1.—: Rotation speeds of the core (dashed lines) and envelope (solid lines) for 3 rotation scenarios, as simulated by our code. Compare with Figure 3 from Gallet & Bouvier (2013).

They fit three prescriptions for  $\tau_c$ : one for the fast rotators, one for the intermediate rotators, and one for the slow rotators. A fast, intermediate, and slow rotator have initial rotation periods of 1.4, 7, and 10 days respectively. The circumstellar disk is assumed to dissipate at 2.5, 5, and 5 Myr respectively. The intermediate and slow rotators have similar evolutions, and similar parameters. For each prescription, we found the  $K$  that reproduces the Sun’s rotation rate at its current age of 4.57 Gyr. All 3 prescriptions are shown in Figure 1, and their parameters are summarized in Table 1.

Prescription	Init $P_{rot}$	$K$	$\tau_c$	$\omega_{sat}$	$T_{disk}$
<i>Fast</i>	1.4	0.155	12	2.45	2.5
<i>Intermediate</i>	7	0.17	28	2.45	5
<i>Slow</i>	10	0.17	30	2.45	5

TABLE 1: Rotation parameters for 3 different prescriptions. Units are days for  $P_{rot}$ , Myr for  $\tau_c$ , and Myr for  $T_{disk}$ .

## 3. SIMULATION METHOD

The simulation code consists of 3 main components: 1. the orbit solver 2. Initial condition solver 3. Fast-rotator estimator

### 3.1. Orbit solver

This code is a revamped and much-improved version of the code written by Penev et al. (2012). The code is described by Penev et al. (2014).

The orbit solver uses the GNU Scientific Library (GSL) to solve the system of ODEs with respect to time. At the beginning of a star’s life, when there is no planet and the radiative zone has yet to form, the convective rotation rate is locked to that of the disk and there is no need for simulation. After the radiative zone forms, we have 2 variables:  $L_{conv}, L_{rad}$ . After the planet also forms, we have 3 variables:  $L_{conv}, L_{rad}, a$ . When the planet dies, we again have only 2 variables. The orbit solver automatically detects which variables are relevant at each timestep, and uses the correct set of differential equations to advance to the next timestep.

To improve both speed and stability, we use GSL’s implicit Bulirsch-Stoer stepper function.

We used  $a^{6.5}$  as the dependent variable instead of  $a$ , because at the end of the planet’s lifetime,  $a$  decreases extremely rapidly with time. This creates accuracy and performance issues with GSL’s ODE solver.  $a^{6.5}$  behaves more nicely because  $\frac{da^{6.5}}{dt}$  does not exhibit the same sensitive dependence on  $a$  as  $\frac{da}{dt}$ .

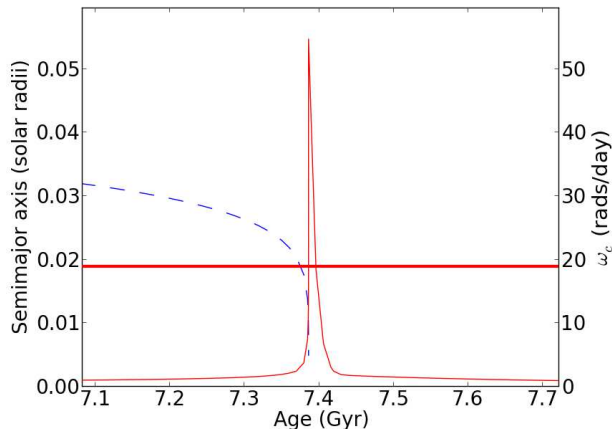


FIG. 2.— HAT-P-20b spiralling into its star. The blue dashed line represents the semimajor axis; the red line represents the star’s rotation rate. The bold red line is the rotation threshold we use,  $P_{rot} = 8h$ .

For illustrative purposes, Figure 2 shows the evolution of semimajor axis and spin rate for one particular stellar system, namely HAT-P-20, as simulated by our code. Notice the huge jump in spin rate after the star swallows its planet, and the rapid decline in spin rate afterwards.

### 3.2. Fast rotator estimator

This portion of the code is run for 3 assumptions about  $Q_*$  ( $10^6, 10^7, 10^8$ ).

The code selects a star of random mass and random initial rotational period, where ‘initial’ means at 5 Myr. It selects a planet with random initial semimajor axis, random radius, and random mass, and puts it in orbit around the star. The orbit solver is then used to evolve the system until the planet passes through the Roche radius, the planet passes through the star’s radius, the star dies, or the maximum age of 10 Gyr is reached, whichever comes first. 10 Gyr is the limit of the YREC stellar models that we use, but since it is also close to the age of the universe, it prevents low-mass stars from living longer than the age of the universe. The Roche radius  $r$  and the lifetime  $l$  are computed using:

$$l = (9Gyr) \left( \frac{M_*}{M_\odot} \right)^{-3}$$

$$r = 2.44r_p \left( \frac{M_*}{m_p} \right)^{1/3}$$

Note that this definition of lifetime is somewhat contrived, since a more accurate expression is  $(10Gyr) \left( \frac{M_*}{M_\odot} \right)^{-2.5}$ . It was chosen purely due to limitations in the YREC tracks, but for masses around 1 solar

mass, it is close to the ‘actual’ main-sequence lifetime. We don’t consider masses above  $1.05M_\odot$ , and low-mass stars have lifetimes above 10 Gyr, so their precise lifetimes are never used.

If the planet is swallowed by the star, which happens if the planet passes the Roche radius or the stellar surface, the orbit solver removes the planet, adds its leftover angular momentum to the star’s convective zone, and continues evolving until 1 or 10 Gyr is reached. It then computes the total amount of time during which the star completes more than 3 revolutions per day. This threshold was chosen so that for all stars in this simulation, the natural evolution of the star (without any tidal effects from the planet) would not cause its rotation speed to exceed the threshold at any point. We assume that the age distribution of stars is uniform, meaning that the probability  $P$  of catching this specific star rotating very fast is proportional to the time it spent rotating very fast, divided by  $\min(1, 10 \text{ Gyr})$ .

We assume that the planet is destroyed instantaneously upon touching the star or passing the Roche radius. Metzger et al. (2012) describes the process of planet destruction and lists three qualitatively different scenarios, depending on the density ratio  $\rho_p/\rho_*$ . If  $1 < \rho_p/\rho_* < 5$ , the planet reaches the Roche radius and stably transfers mass to the star over a timescale of thousands of years. If the density ratio is lower, the planet still reaches the Roche radius, but quickly breaks up and accretes onto the star on a timescale of days to weeks. If the density ratio is higher, the planet plunges into the stellar atmosphere and is destroyed in about 100 days. Since even 1000 years is negligible compared to the megayear timescales that fast rotation rates are expected to last, our approximation of instantaneous accretion is very safe.

This process of picking a random star and random planet is repeated until 10,000 stars exceed the threshold of  $P_{rot} = 8h$  due to the death of their planets. Intermediate results are printed out to make sure the results converge.

Every aspect of this random sampling process will now be discussed.

#### 3.2.1. Stellar mass distribution

The mass distribution is taken from the Kepler Target Catalog, which are the stars in the Kepler Input Catalog selected for examination by Kepler. We take the mass distribution from Kepler because it is a convenient catalog of stellar information, and because it is meant to catalogue Sun-like stars—not too dissimilar to the stars present and future transit surveys focus on.

Stars with a mass less than 0.5 or more than  $1.05 M_\odot$  were excluded. A bin is randomly selected according to a histogram representing the distribution. The stellar mass is then chosen uniformly at random between the two bin edges. For example, if the bin (0.5, 0.506) is chosen, the mass is chosen from the range 0.5–0.506 with uniform probability.

#### 3.2.2. Planetary orbit distribution

Howard et al. (2012) uses Kepler data to derive the current distribution of planets with respect to their period  $P$  and their radius  $R$ . The distributions they found

were:

$$\frac{df}{d\log P} \propto P^\beta (1 - e^{-\gamma \frac{P}{P_0}})$$

$$\frac{df}{d\log R} \propto R^\alpha$$

$\frac{df}{d\log P}$  is the fraction of planets in a logarithmic interval centered on  $P$ .  $\alpha = -1.92$ .  $\beta$ ,  $\gamma$ , and  $P_0$  depend on radius, but we only consider planets with radii greater than  $8 R_\oplus$ . This is because planets significantly below this radius are not hot Jupiters, and are unlikely to have the mass necessary to significantly influence their stars' rotation rates. For this radius range ( $8\text{--}32 R_\oplus$ ),  $\beta = 0.37 \pm 0.35$ ,  $P_0 = 1.7 \pm 0.7$ , and  $\gamma = 4.1 \pm 2.5$ . Additionally, we also only consider planets with a period less than 5.9 days, under the assumption that planets with longer periods will not inspiral into their stars.

Note that these distributions are for currently-observed planets, whereas we want the period distribution when the planets first formed. To get the latter from the former, we first assume that the initial distribution be represented with the same 3 parameters:  $\beta, P_0, \gamma$ . We created an algorithm which takes these 3 initial parameters, randomly samples planets from that distribution, and evolves them for a random amount of time. The resulting distribution is compared to the modern-day distribution using the KS test—the lower the KS statistic, the better the fit. A simulated annealing algorithm was used to sample the 3-dimensional parameter space and find the best initial distribution for every  $Q$ . The results are presented in Table 2.

$Q_*$	$\beta$	$P_0$	$\gamma$
$10^6$	-1.4	1.1	16.3
$10^7$	0.088	1.5	16.2
$10^8$	0.44	1.6	4.1

TABLE 2: Initial orbital period distributions

### 3.2.3. Planetary mass distribution

We assume that the planetary mass distribution is independent of radius. For hot Jupiters ( $R > 8R_\oplus$ ), this is roughly true, as shown by exoplanets.org data and well-supported by theory.

The mass distribution we use was taken from exoplanets.org. Only planets discovered by transit searches with a radius greater than  $8 R_\oplus$ , a period smaller than 5.9 days, and a known mass were included. For hot Jupiters, detection probability is not highly correlated with radius. It is however highly correlated with orbital period—even for periods as short as 5.9 days, longer-period planets are much less likely to be detected. However, since we are making the assumption that orbital period is not highly correlated with radius or mass for this radius range—the same assumption that Howard et al. (2012) make due to lack of data—there is no need to correct for observational biases.

A bin is randomly selected according to the distribution in the histogram. The planet mass is then chosen uniformly at random between the two bin edges. The algorithm is exactly the same as the one used for selecting stellar masses.

### 3.2.4. Stellar rotation distribution

This distribution is taken from Irwin et al. (2008) for the open cluster NGC 2362, which is 5 Myr old.

The data is histogrammed into 10 bins. A random rotational period is generated by taking the star's mass, finding its corresponding bin, randomly choosing one of the stars in the bin, and returning its rotation rate.

We always choose  $K$  and  $\tau_c$  based on this randomly-chosen rotation rate. Whichever prescription the star's initial rotation rate is closest to in Table 1, the corresponding parameters are chosen and used throughout the evolution.

## 4. RESULTS AND DISCUSSION

According to Fressin et al. (2013), the rate of hot Jupiters per star is 0.00252. With this number, we get the results in Table 3.

$Q_*$	Stellar fraction	Sensitivity	Destruction rate
$10^6$	$2.9 \times 10^{-6}$	0.21	0.92
$10^7$	$0.35 \times 10^{-6}$	0.52	0.37
$10^8$	$0.08 \times 10^{-6}$	0.81	0.083

TABLE 3: Results of 3 simulations, for 3 different values of  $Q_*$ , each of which ran until 10,000 modern-day planets were simulated. Each simulation was checked for convergence, and all converged long before the end of the simulation. Second column: fraction of stars that should be rotating faster than  $P_{rot} < 8h$ ; third column: fraction of planet deaths that cause their stars' rotation rates to exceed the threshold; final column: fraction of initial hot Jupiters that are subsequently destroyed

In Figure 3 we show the distribution of stellar ages at which the star spins faster than 8h due to planetary death. Notice that for higher  $Q_*$ , the distribution is broader and shifted towards higher ages. This is because the initial orbital period distribution has fewer short-period planets for high  $Q_*$ , whereas it exhibits a strong peak at low periods for small  $Q_*$ . Also notice the spikes at large ages. These are artifacts, due to the small length of time for which stars rotate quickly after planet death. Because the graphs were constructed by adding up contributions from every dying planet, there are some stellar ages that few stars happened to hit when they were spinning quickly.

In Figure 4 we show the distribution of times after planet death at which the star is spinning quickly. For example, one can tell that most stars are still spinning quickly 5 Myr after planet death, whereas after 20 Myr, almost all stars have spun down. Notice that a small but non-zero percentage of values are negative. This is because some planets spin up their stars before dying, while most only spin up their stars after dying and depositing their angular momentum onto the star's surface. Notice also that the distribution is broader for higher  $Q_*$ . This is because a planet that formed at higher semimajor axis has more angular momentum, and therefore deposits more angular momentum onto the star. Since the initial period distribution has more short-period planets for low  $Q_*$ , the average dying planet deposits less angular momentum, thereby creating a narrower peak in Figure 4.

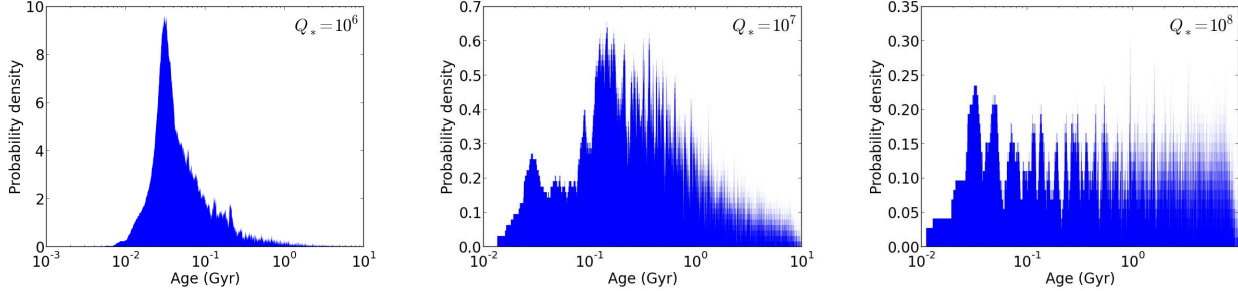


FIG. 3.—: Distribution of stellar ages at which the star’s spin rate exceeded threshold due to planet death.

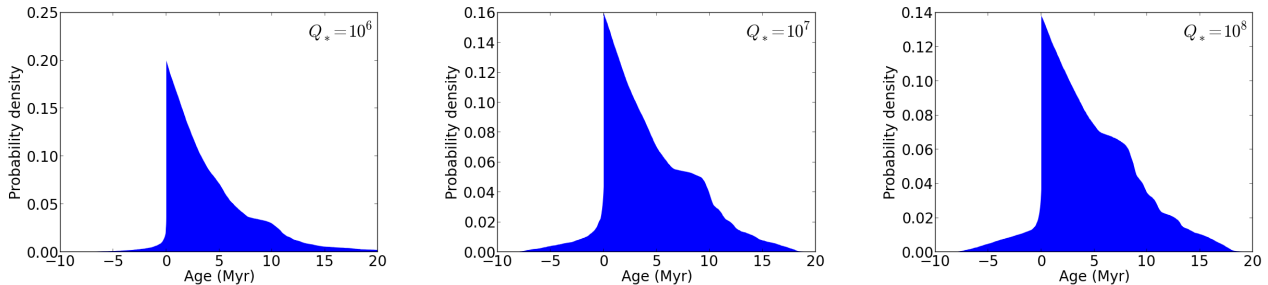


FIG. 4.—: These plots represent the fraction of threshold-exceeding stars that still exceed the rotation threshold ( $P < 8h$ ) at a certain age after planet death.

Index	$\beta$	$P_0$	$\gamma$
0	0.37	1.7	4.1
1	0.02	1.7	4.1
2	0.72	1.7	4.1
3	0.37	1.0	4.1
4	0.37	2.4	4.1
5	0.37	1.7	1.6
6	0.37	1.7	6.5

TABLE 4: Modern orbital period distributions used to test sensitivity. 0 is nominal.

#### 4.1. Sensitivity of results

The modern period distribution for exoplanets is highly uncertain. We have assumed the period distribution given in Howard et al. (2012), which has 3 parameters:  $\beta, P_0, \gamma$ . Their values and uncertainties are  $\beta = 0.37 \pm 0.35$ ,  $P_0 = 1.7 \pm 0.7$ , and  $\gamma = 4.1 \pm 2.5$ . To test the sensitivity of our results, we have run our simulation assuming 6 different combinations of these 3 parameters, meant to explore the extremes of every parameter. The combinations are given in Table 4.

For each of the six modern orbital period distributions and each of the three  $Q_*$ , we found the initial distribution and ran a simulation to find the fraction of stars expected to be rotating quickly. The results are shown in Table 5. Notice that the differences between assumed modern period distributions, for every  $Q_*$ , are within an order of magnitude—significantly below the uncertainty in  $Q_*$ .

#### 4.2. Detectability of fast rotators

Recently, McQuillan et al. (2014) used an autocorrelation algorithm on the light curves of 133,030 main-sequence Kepler stars and detected rotation periods for 34,030 (25.6%). The detected rotation periods ranged from 0.2 to 70 days—the former showing that such extreme rotation periods are possible and detectable. The

Index	$Q_*$	Stellar fraction $\times 10^6$
0	$10^6$	2.9
0	$10^7$	0.35
0	$10^8$	0.08
1	$10^6$	10
1	$10^7$	0.61
1	$10^8$	0.106
2	$10^6$	3.60
2	$10^7$	0.346
2	$10^8$	0.067
3	$10^6$	12.7*
3	$10^7$	2.14*
3	$10^8$	0.36
4	$10^6$	1.67
4	$10^7$	0.26
4	$10^8$	0.047
5	$10^6$	15*
5	$10^7$	1.07*
5	$10^8$	0.3
6	$10^6$	4.6
6	$10^7$	0.32
6	$10^8$	0.068

TABLE 5: Stellar fraction of fast rotators for every modern orbital period distribution and every  $Q_*$ . Results marked with \* are unreliable because no initial period distribution could be found that closes matches the modern distribution. In such cases, the closest match was used to compute the result. 0 is the nominal scenario.

authors report a typical range of rotation-induced amplitudes of 950–22,700 ppm, with a median of 5600 ppm. The amplitude is highly dependent on both period and temperature, with cool quickly-rotating stars having a much larger amplitude than hot quickly-rotating stars. For comparison, HATNet (Bakos et al. (2004)) is capable of 2 mmag (1800 ppm) photometry on bright stars, with 6 mmag (5500 ppm) being a more typical precision.

Thus, HATnet and similar exoplanet surveys should be capable of measuring rotation periods for roughly 13% of the nearby analogues of Kepler main sequence stars.

This 25.6% detection rate does not pose as much of a problem to detecting planet-swallowing stars with  $P < 8h$  as might be expected. Survey biases heavily favor detecting low rotation periods. A low rotation period would mean that a given observation timeframe spans many more periods, giving a stronger signature and reducing the effects of systematic biases that vary with time. Starspots and other features also change much less from one period to the next if the period is 8 hours instead of weeks, giving a more strongly periodic signal.

It should be noted that the detection rate in McQuillan et al. (2014) depended heavily on temperature. When they divided stars into temperature bins, they found that the lowest temperature bin ( $< 4000K$ ) had a 83% detection rate. They suggested that misalignment between the star’s equator and our line of sight could account for some of the remaining 17%. Their next-lowest bin (4000-4500 K) has a detection rate of 69%, and 4000K corresponds roughly to the 0.5 solar masses that is the lower mass limit of our study.

It should also be noted that many authors have already used light curves from ground-based transit surveys to measure stellar rotation rates in clusters. For example, Collier Cameron et al. (2009) reports rotation rates in the 600 Myr Coma Berenices open cluster using SuperWASP data, while Delorme et al. (2011) similarly uses SuperWASP to measure two other clusters of similar age: Hyades and Praesepe. Hartman et al. (2010) examined Pleiades members between 0.4 and 1.3 solar masses and detected rotation periods for 74 percent of stars within the field of view. This detection rate increased to 93 percent for stars between 0.7 and 1.0 solar masses. Of course, it is easier to detect rotation in cluster stars than in field stars because young stars have shorter rotation periods and are more variable. Nevertheless, fast rotators—aside from being easier to detect—are expected to exhibit higher-amplitude variations due to higher magnetic activity. This is shown observationally (McQuillan et al. (2014), Noyes et al. (1984)) and expected from stellar dynamo theory (Parker (1955)) since faster rotation produces a stronger magnetic field, which in turn results in higher stellar activity. For example, Karak et al. (2014) demonstrate quantitatively, by extending the solar flux transport dynamo model to other stars, that the toroidal flux amplitude increases with rotation. They note that this explains the general trend of Ca II H/K and X-ray observations, which are signatures of magnetic activity.

A final concern is that even though the simulation predicts very fast rotation rates, such rates may exceed the breakup speed of the star and hence be unphysical. We do not take this into consideration in our simulation, as a detailed examination of the physics of extreme stellar rotation is outside the scope of this paper. However, we note that there is no possibility of planetary accretion causing the star’s envelope to reach escape velocity—after all, the planet itself is in a tight orbit when it breaks up. Qualitatively, we expect the stellar envelope to expand and become more oblate, increasing its moment of inertia and decreasing its rotation speed until it no longer exceeds the breakup speed. We also note that the breakup

period of the Sun is 2.8 hours—significantly below the 8-hour limit used in this paper—and that the majority of stars in our simulation never reach the breakup period.

## 5. CONCLUSIONS

We have simulated the tidal decay of hot Jupiters for 3 different values of  $Q_*$ :  $10^6$ ,  $10^7$ ,  $10^8$ . We find that, within an order of magnitude, one out of a million Sun-like stars are expected to exhibit rotation periods less than 8h as a result of swallowing a planet. Ground-based exoplanet surveys have examined millions of stars, but only a fraction may exhibit enough variability to find even a very fast rotation period. Thus, we conclude that it is possible for these surveys to detect a fast rotator if  $Q_* = 10^6$ , but unlikely if  $Q_* = 10^8$  or greater.

A very fast rotation rate is a good indicator because 20-80 percent of hot Jupiter deaths (depending on  $Q_*$ ) cause their host stars to spin faster than  $P_{rot} < 8h$ , and because there are very few other explanations of such a high rotation rate:

1. The star is young (pre-main-sequence or near ZAMS)
2. Tidal interaction in a binary system

Scenario 2 can usually be excluded because huge Doppler shifts, anomalous spectra, and/or transits are all easily detectable features of binary systems, where ‘easily detectable’ is with respect to the ease of detecting a planetary transit. Scenario 1 is harder to exclude because it is extremely hard to date stars.

Other observations may enable confirmation that a planet was tidally destroyed. Observing the rocky core is the most direct method, providing that the planet was not destroyed through a direct-impact merger and that the tidal disruption process was not violent enough to destroy the core. If the core is not detectable, there may be detectable changes in stellar metallicity. Théado & Vauclair (2012) analyzed the change in stellar metallicity due to accretion of protoplanetary disk material, and found that accretion of a Jupiter-mass planet can cause changes in the relative metal abundances in the star’s convective zone that last on the order of tens of Myr. It is not clear whether these changes are practically observable, especially given the broadening of spectral lines caused by the extreme rotation.

## REFERENCES

- Adamów, M., Niedzielski, A., Villaver, E., Nowak, G., & Wolszczan, A. 2012, *ApJ*, 754, L15
- Albrecht, S., Winn, J. N., Johnson, J. A., Howard, A. W., Marcy, G. W., Butler, R. P., Arriagada, P., Crane, J. D., Shectman, S. A., Thompson, I. B., Hirano, T., Bakos, G., & Hartman, J. D. 2012, *ApJ*, 757, 18
- Allain, S. 1998, *A&A*, 333, 629
- Bakos, G., Noyes, R. W., Kovács, G., Stanek, K. Z., Sasselov, D. D., & Domsa, I. 2004, *PASP*, 116, 266
- Bakos, G. Á., Csabry, Z., Penev, K., Bayliss, D., Jordán, A., Afonso, C., Hartman, J. D., Henning, T., Kovács, G., Noyes, R. W., Béky, B., Suc, V., Csák, B., Rabus, M., Lázár, J., Papp, I., Sári, P., Conroy, P., Zhou, G., Sackett, P. D., Schmidt, B., Mancini, L., Sasselov, D. D., & Ueltzhoeffer, K. 2013, *PASP*, 125, 154
- Barker, A. J. & Ogilvie, G. I. 2009, *MNRAS*, 395, 2268
- Barnes, S. & Sofia, S. 1996, *ApJ*, 462, 746
- Collier Cameron, A., Davidson, V. A., Hebb, L., Skinner, G., Anderson, D. R., Christian, D. J., Clarkson, W. I., Enoch, B., Irwin, J., Joshi, Y., Haswell, C. A., Hellier, C., Horne, K. D., Kane, S. R., Lister, T. A., Maxted, P. F. L., Norton, A. J., Parley, N., Pollacco, D., Ryans, R., Scholz, A., Skillen, I., Smalley, B., Street, R. A., West, R. G., Wilson, D. M., & Wheatley, P. J. 2009, *MNRAS*, 400, 451
- Counselman, III, C. C. 1973, *ApJ*, 180, 307
- Delorme, P., Cameron, A. C., Hebb, L., Rostron, J., Lister, T. A., Norton, A. J., Pollacco, D., & West, R. G. 2011, in *Astronomical Society of the Pacific Conference Series*, Vol. 448, 16th Cambridge Workshop on Cool Stars, Stellar Systems, and the Sun, ed. C. Johns-Krull, M. K. Browning, & A. A. West, 841
- Demarque, P., Guenther, D. B., Li, L. H., Mazumdar, A., & Straka, C. W. 2008, *Ap&SS*, 316, 31
- Fressin, F., Torres, G., Charbonneau, D., Bryson, S. T., Christiansen, J., Dressing, C. D., Jenkins, J. M., Walkowicz, L. M., & Batalha, N. M. 2013, *ApJ*, 766, 81
- Gallet, F. & Bouvier, J. 2013, *A&A*, 556, A36
- Goldreich, P. 1963, *MNRAS*, 126, 257
- Hartman, J. D., Bakos, G. Á., Kovács, G., & Noyes, R. W. 2010, *MNRAS*, 408, 475
- Hebb, L., Collier-Cameron, A., Triaud, A. H. M. J., Lister, T. A., Smalley, B., Maxted, P. F. L., Hellier, C., Anderson, D. R., Pollacco, D., Gillon, M., Queloz, D., West, R. G., Bentley, S., Enoch, B., Haswell, C. A., Horne, K., Mayor, M., Pepe, F., Segransan, D., Skillen, I., Udry, S., & Wheatley, P. J. 2010, *ApJ*, 708, 224
- Hellier, C., Anderson, D. R., Collier Cameron, A., Gillon, M., Hebb, L., Maxted, P. F. L., Queloz, D., Smalley, B., Triaud, A. H. M. J., West, R. G., Wilson, D. M., Bentley, S. J., Enoch, B., Horne, K., Irwin, J., Lister, T. A., Mayor, M., Parley, N., Pepe, F., Pollacco, D. L., Segransan, D., Udry, S., & Wheatley, P. J. 2009, *Nature*, 460, 1098
- Hellier, C., Anderson, D. R., Collier-Cameron, A., Miller, G. R. M., Queloz, D., Smalley, B., Southworth, J., & Triaud, A. H. M. J. 2011, *ApJ*, 730, L31
- Howard, A. W., Marcy, G. W., Bryson, S. T., Jenkins, J. M., Rowe, J. F., Batalha, N. M., Borucki, W. J., Koch, D. G., Dunham, E. W., Gautier, III, T. N., Van Cleve, J., Cochran, W. D., Latham, D. W., Lissauer, J. J., Torres, G., Brown, T. M., Gilliland, R. L., Buchhave, L. A., Caldwell, D. A., Christensen-Dalsgaard, J., Ciardi, D., Fressin, F., Haas, M. R., Howell, S. B., Kjeldsen, H., Seager, S., Rogers, L., Sasselov, D. D., Steffen, J. H., Basri, G. S., Charbonneau, D., Christiansen, J., Clarke, B., Dupree, A., Fabrycky, D. C., Fischer, D. A., Ford, E. B., Fortney, J. J., Tarter, J., Girouard, F. R., Holman, M. J., Johnson, J. A., Klaus, T. C., Machalek, P., Moorhead, A. V., Morehead, R. C., Ragozzine, D., Tenenbaum, P., Twicken, J. D., Quinn, S. N., Isaacson, H., Shporer, A., Lucas, P. W., Walkowicz, L. M., Welsh, W. F., Boss, A., Devore, E., Gould, A., Smith, J. C., Morris, R. L., Prsa, A., Morton, T. D., Still, M., Thompson, S. E., Mullally, F., Endl, M., & MacQueen, P. J. 2012, *ApJS*, 201, 15
- Irwin, J. & Bouvier, J. 2009, in *IAU Symposium*, Vol. 258, *IAU Symposium*, ed. E. E. Mamajek, D. R. Soderblom, & R. F. G. Wyse, 363–374
- Irwin, J., Hodgkin, S., Aigrain, S., Bouvier, J., Hebb, L., Irwin, M., & Moraux, E. 2008, *VizieR Online Data Catalog*, 738, 40675
- Jackson, B., Greenberg, R., & Barnes, R. 2008, *ApJ*, 678, 1396
- Jackson, B., Miller, N., Barnes, R., Raymond, S. N., Fortney, J. J., & Greenberg, R. 2010, *MNRAS*, 407, 910
- Jackson, B., Stark, C. C., Adams, E. R., Chambers, J., & Deming, D. 2013, *ApJ*, 779, 165
- Karak, B. B., Kitchatinov, L. L., & Choudhuri, A. R. 2014, *ArXiv e-prints*
- Kaula, W. M. 1968, *An introduction to planetary physics - The terrestrial planets*, ed. Kaula, W. M.
- Kawaler, S. D. 1988, *ApJ*, 333, 236
- MacGregor, K. B. 1991, in *NATO ASIC Proc. 340: Angular Momentum Evolution of Young Stars*, 315–+
- McQuillan, A., Mazeh, T., & Aigrain, S. 2013, *ApJ*, 775, L11
- . 2014, *ApJS*, 211, 24
- Meibom, S. & Mathieu, R. D. 2005, in *Astronomical Society of the Pacific Conference Series*, Vol. 333, *Tidal Evolution and Oscillations in Binary Stars*, ed. A. Claret, A. Giménez, & J.-P. Zahn, 95
- Metzger, B. D., Giannios, D., & Spiegel, D. S. 2012, *MNRAS*, 425, 2778
- Noyes, R. W., Hartmann, L. W., Baliunas, S. L., Duncan, D. K., & Vaughan, A. H. 1984, *ApJ*, 279, 763
- Ogilvie, G. I. & Lin, D. N. C. 2007, *ApJ*, 661, 1180
- Parker, E. N. 1955, *ApJ*, 122, 293
- Penev, K., Jackson, B., Spada, F., & Thom, N. 2012, *ApJ*, 751, 96
- Penev, K. & Sasselov, D. 2011, *ApJ*, 731, 67
- Penev, K., Zhang, M., & Jackson, B. 2014, *ArXiv e-prints*
- Pepper, J., Pogge, R. W., DePoy, D. L., Marshall, J. L., Stanek, K. Z., Stutz, A. M., Poindexter, S., Siverd, R., O'Brien, T. P., Trueblood, M., & Trueblood, P. 2007, *PASP*, 119, 923
- Plavchan, P. & Bilinski, C. 2013, *ApJ*, 769, 86
- Rasio, F. A., Tout, C. A., Lubow, S. H., & Livio, M. 1996, *ApJ*, 470, 1187
- Stauffer, J. R. & Hartmann, L. W. 1987, *ApJ*, 318, 337
- Street, R. A. & SuperWASP Consortium. 2004, *Baltic Astronomy*, 13, 707
- Teitler, S. & Königl, A. 2014, *ArXiv e-prints*
- Théado, S. & Vauclair, S. 2012, *ApJ*, 744, 123
- Winn, J. N., Fabrycky, D., Albrecht, S., & Johnson, J. A. 2010, *ApJ*, 718, L145